archives
of thermodynamics
Vol. **39**(2018), No. 3, 45–61
DOI: 10.1515/aoter-2018-0019

Investigation of thermal interactions between elements of propulsion system and selected parts of the airplane skin in small aircrafts

PIOTR ŁAPKA*
MIROSŁAW SEREDYŃSKI
PIOTR FURMAŃSKI

Institute of Heat Engineering, Warsaw University of Technology,
Nowowiejska 21/25, 00-665 Warsaw

Abstract Development of new or upgrading of existing airplanes requires many different analyses, e.g., thermal, aerodynamical, structural, and safety. Similar studies were performed during re-design of two small aircrafts, which were equipped with new turboprop engines. In this paper thermo-fluid analyses of interactions of new propulsion systems with selected elements of airplane skin were carried out. Commercial software based numerical models were developed. Analyses of heat and fluid flow in the engine bay and nacelle of a single-engine airplane with a power unit in the front part of the fuselage were performed in the first stage. Subsequently, numerical simulations of thermal interactions between the hot exhaust gases, which leave the exhaust system close to the front landing gear, and the bottom part of the fuselage were investigated. Similar studies were carried out for the twin-engine airplane with power units mounted on the wings. In this case thermal interactions between the hot exhaust gases, which were flowing out below the wings, and the wing covers and flaps were studied. Simulations were carried out for different airplane configurations and operating conditions. The aim of these studies was to check if for the assumed airplane skin materials and the initially proposed airplane geometries, the cover destruction due to high temperature is likely. The results of the simulations were used to recommend some modifications of constructions of the considered airplanes.

*Corresponding Author. Email: piotr.lapka@itc.pw.edu.pl

Keywords: Computational fluid dynamics; Numerical heat transfer; Propulsion system; Small aircraft; Thermal interactions

Nomenclature

c_p	–	specific heat, J/kg/K
C_1, C_μ	–	variables in the k-ϵ turbulence model
C_2, $C_{1\varepsilon}$, $C_{3\varepsilon}$	–	constants in the k-ϵ turbulence model
D	–	diffusion coefficient, m^2/s
G_b, G_k	–	generation of turbulent kinetic energy due to buoyancy and mean velocity gradients
h	–	volumetric enthalpy, J/m^3
I	–	thermal radiation intensity, $W/m^2/sr$
J	–	mass diffusion flux, m/s
k	–	turbulent kinetic energy, J/kg
K_a	–	absorption coefficient, 1/m
n	–	refractive index
p	–	pressure, Pa
Pr_t	–	turbulent Prandtl number
q_r	–	radiative heat flux, W/m^2
s	–	path of radiation propagation, m
S	–	variable in the k-ϵ turbulence model
Sc_t	–	turbulent Schmidt number
T	–	temperature, K
u_i	–	mean velocity component, m/s
Y	–	mass fraction

Greek symbols

δ_{ij}	–	Kronecker delta
ε	–	turbulence dissipation rate, J/kg/s
λ, λ_t	–	molecular and turbulent thermal conductivity, W/m/K
μ, μ_t	–	dynamic and turbulent (eddy) viscosities, Pa s
ν	–	kinematic viscosity, m^2/s
ρ	–	density, kg/m^3
σ	–	blackbody constant, $W/m^2/K^4$
σ_k, σ_ε	–	turbulent Prandtl numbers for k and ε

Subscripts

m	–	number of species

1 Introduction

During development of new aircrafts or re-designing of the existing constructions many technical problems have to be solved to ensure safety exploitation of the airplanes [1–8]. Moreover, operations of many systems

and equipment, e.g., propulsion system, fuels supply system, cooling and ventilation systems, avionics equipment, steering system and many others should be carefully analysed in the most adverse conditions. Also their influence on the other elements of the aircraft should be checked. Similar studies were performed during development of a new version of two small aircrafts I-23 and EV-55 which were equipped in new turboprop engines [1–7]. Among them thermal interaction of the selected elements of propulsion systems with the airplane skin were also investigated [3,5–7]. These analyses led to several design recommendation and modifications of initially proposed geometries of nacelles and airplane skins.

This paper summaries thermo-fluid numerical investigations performed during re-development of the two small airplans under the FP7 EU ESPOSA project (Efficient Systems and Propulsion for Small Aircraft) [3,5–7]. At first both airplanes are briefly presented and then the thermo-fluid models are shown in more details. Subsequently, the preliminary numerical simulations of fluid flow and heat transfer inside the engine bay and in the composite nacelle of the I-23 are presented and discussed. Then investigations of thermal interaction of exhaust jets with a fuselage of the single-engine airplane and with wings and flaps of the twin-engine airplane are presented and the results obtained analysed. Finally, recommendation for modification of the initial airplane geometries are given.

2 Description of the airplanes under consideration

Both airplanes are in the tractor configuration and are shown in Fig. 1. The single-engine airplane I-23 (Fig. 1A) has a turboprop engine located in the front part of the fuselage. The new power unit replaced the old piston one. The new type of propulsion leads to a completely new design of the cowling, engine bay and all systems located inside the nacelle – see Fig. 2A. The proposed new nacelle is made of composite materials (honeycomb structure and solid laminate) with the maximum allowable temperature of operation not exceeding 433 K. Above this temperature the cowling material starts to soften. In this plane the exhaust system directs the exhaust gases outside the airplane through two symmetrical curved pipes (Figs. 1A and 2B). The outlets of exhaust system are located below the front part of the fuselage, therefore streams of hot exhaust gases may thermally interact with bottom parts of the airplane cover. The exhaust outlet ducts are covered with some

shielding pipes (see Fig. 2A) and through the gap between the exhaust pipe and their cover the air is sucked in from the nacelle due to the ejector effect. This additional flow of the cold air decreases the exhaust system temperature and enhances the engine bay ventilation.

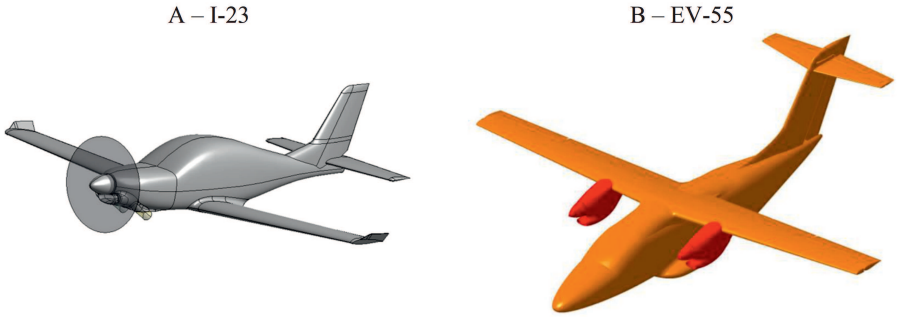

Figure 1: Airplanes: A) single-engine I-23 with the engine in the fuselage and B) twin-engine EV-55 with engines on the wings.

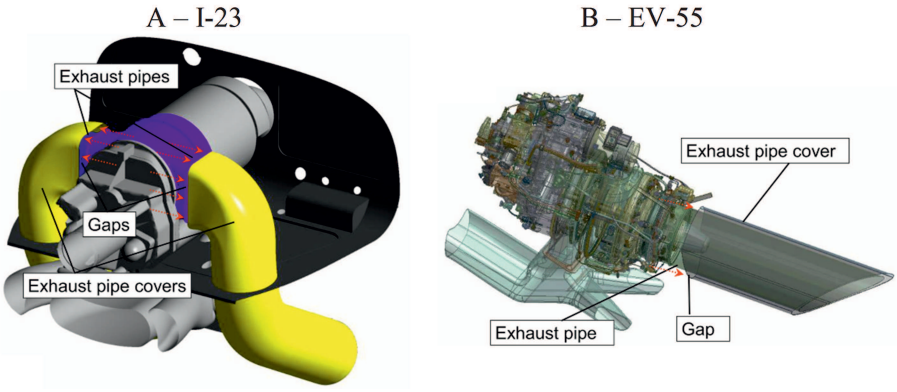

Figure 2: Power unit, engine bay and exhaust system of the: A) I-23 and B) EV-55.

The upgraded twin-engine airplane EV-55 is equipped with two turboprop engines located on the wings (Fig. 1B). The power unit with equipment and exhaust system is shown in Fig. 2B. The nacelle and airplane skin (wings and flaps) of this aircraft are made of a solid laminate – glass fabric-epoxy prepreg which has the maximum allowed operation temperature equal to 393 K. In the airplane exhaust gases flow out to the environment through the short straight pipe (Fig. 2B) which outlet is located at the back of the engine bay below and parallel to the wing surface. There is also a gap

between the exhaust pipe and its cover through which the cold air is sucked in from the engine bay due to the ejector effect. Similarly as for the I-23 this additional air flow cools down the exhaust system and improves ventilation of the engine bay. Outside the airplane the hot exhaust gases are flowing below and close to the wings and therefore may thermally interact with them and with flaps, especially when the flaps are in the fully extended position.

3 Numerical models

During all simulations turbulent and incompressible fluid flow was assumed due to low values of Mach number. In the analyses of fluid flow and heat transfer in the engine bay and nacelle conductive and convective heat transfer in the nacelle solid parts and in the flowing air, respectively were assumed. Moreover, thermal radiation between hot engine and cold nacelle grey surfaces was accounted for with the air treated as the transparent medium. In the analyses of exhaust gases interactions with the airplanes skin conductive and convective heat transfer modes were also considered. Moreover, the exhaust gases composition was accounted for to include absorption and emission of thermal radiation by hot gas components.

The steady state forms of Reynolds averaged continuity and momentum equations were assumed as follows [9]:

$$\frac{\partial u_j}{\partial x_j} = 0 \,, \tag{1}$$

$$\rho \frac{\partial \left(u_i u_j\right)}{\partial x_j} = -\frac{\partial p}{\partial x_i} + \frac{\partial}{\partial x_j}\left[\mu\left(\frac{\partial u_i}{\partial x_j} + \frac{\partial u_j}{\partial x_i}\right)\right] + \frac{\partial}{\partial x_j}\left[\mu_t\left(\frac{\partial u_i}{\partial x_j} + \frac{\partial u_j}{\partial x_i}\right) - \frac{2}{3}\rho k \delta_{ij}\right] \,, \tag{2}$$

where: k – turbulent kinetic energy, p – pressure, u_i – mean velocity component, δ_{ij} – Kronecker delta, μ and μ_t – dynamic and turbulent (eddy) viscosities, respectively, and ρ – density. The following realizable k-ε turbulence model with the scalable wall function approximation was applied to account for turbulent flow [9]:

$$\rho \frac{\partial \left(k u_j\right)}{\partial x_j} = \frac{\partial}{\partial x_j}\left[\left(\mu + \frac{\mu_t}{\sigma_k}\right)\frac{\partial k}{\partial x_j}\right] + G_k + G_b - \rho\varepsilon \,, \tag{3}$$

$$\rho\frac{\partial\left(\varepsilon u_j\right)}{\partial x_j}=\frac{\partial}{\partial x_j}\left[\left(\mu+\frac{\mu_t}{\sigma_\varepsilon}\right)\frac{\partial\varepsilon}{\partial x_j}\right]+\rho C_1 S\varepsilon-\rho C_2\frac{\varepsilon^2}{k+\sqrt{\nu\varepsilon}}+C_{1\varepsilon}\frac{\varepsilon}{k}C_{3\varepsilon}G_b\ , \tag{4}$$

where: C_1 – model variable, C_2, $C_{1\varepsilon}$, and $C_{3\epsilon}$ – model constants, G_b – generation of turbulent kinetic energy due to buoyancy, G_k – generation of turbulent kinetic energy due to the mean velocity gradients, S – model variable, ε – turbulence dissipation rate, ν – kinematic viscosity, σ_k and σ_ε – turbulent Prandtl numbers for k and ε, respectively. In this model the turbulent viscosity is given by $\mu_t=\rho C_\mu k^2/\varepsilon$, where C_μ is the model variable. Default values of all constants in the realizable k-ε turbulence model were assumed in all simulations [9]. Considering species transport and thermal radiation in the participating medium (hot exhaust gases) the energy equation for incompressible turbulent flow assumed the following form:

$$u_j\frac{\partial h}{\partial x_j}=\frac{\partial}{\partial x_j}\left[\left(\lambda+\lambda_t\right)\frac{\partial T}{\partial x_j}-\sum_m h_m J_m\right]-\frac{\partial q_r}{\partial x_j}\ , \tag{5}$$

where: h – volumetric enthalpy, J_m – mass diffusion flux of mth species, m – number of species, q_r – radiative heat flux, T – temperature, λ – molecular thermal conductivity, λ_t – turbulent thermal conductivity ($\lambda_t=c_p\mu_t/\mathrm{Pr}_t$, where: c_p – specific heat, $\mathrm{Pr}_t=0.85$ – turbulent Prandtl number). The viscous dissipation term in Eq. (5) was neglected due to low values of Mach and Brinkman numbers for considered cases and assumed incompressible flow. The conservation equation for species transfer took the following general form:

$$\rho u_j\frac{\partial Y_m}{\partial x_j}=\frac{\partial}{\partial x_j}\left[-\left(\rho D_{m,n}+\frac{\mu_t}{\mathrm{Sc}_t}\right)\frac{\partial Y_m}{\partial x_j}\right]\ , \tag{6}$$

where: $D_{m,n}$ is the diffusion coefficient, Sc_t – turbulent Schmidt number ($\mathrm{Sc}_t=0.7$) and Y_m – mass fraction of mth species. Assuming that the hot exhaust gases were absorbing and emitting thermal radiation with the radiation scattering neglected, the radiation intensity, I, was determined from the following radiative transfer equation [10–12]:

$$\frac{dI}{ds}=-K_a I+\frac{n^2\sigma K_a T^4}{\pi}\ , \tag{7}$$

where: K_a – absorption coefficient, n – refractive index, s – propagation path of thermal radiation, σ – blackbody constant. During the simulations of fluid flow and heat transfer in the engine bay radiative heat transfer

occurred only between grey opaque surfaces which were assumed to be diffusely emitting and reflecting thermal radiation. The air was treated as transparent media ($K_a = 0$). During simulations of thermal interactions of the exhaust jet with airplane skin the weighted sum of grey gases model (WSGGS) [10] was used to find the absorption coefficient of the exhaust gases (assumed as a mixture of nitrogen, oxygen, water vapour and carbon dioxide with the presence of carbon monoxide and soot neglected). The species mass fractions of exhaust gases leaving the engine were estimated based on the assumption of the complete combustion as well as on the composition of the aviation fuel Jet A and the air mass flow rates flowing through the engines at different altitudes and airplane speeds, see [6,7].

The presented mathematical models were subsequently solved by using numerical models developed in the commercial Ansys Workbench environment. The computational domains were created in the DesignModeler. Then the control volume meshes were generated in the ICEM CFD or Ansys Meshing and finally numerical simulations were carried out in the Ansys Fluent. More details related to presented numerical models, boundary conditions, material properties, computational methodology, generated meshes, etc. can be found in the reference papers [3,5–7]. Here only brief summary is given.

The simulation strategy for the engine bay cooling and ventilation was following. In the first step the temperature and velocity fields were found assuming no thermal radiation present in the system. Then in the second step these fields were updated with thermal radiation. This two-step procedure increased convergence rate and reduced time of simulations. The analyses of the exhaust jet thermal interactions with airplane skin were divided into two parts. Distributions of temperature, velocity, turbulent kinetic energy, turbulent dissipation rate and species concentrations at the exhaust outlets as well as velocity, turbulent kinetic energy and turbulent dissipation rate of the wind at inlet for ground simulations were first determined in separated analyses. Then the obtained inlet profiles were applied as boundary conditions for main simulations of heat and fluid flow over the body of airplanes on the ground and in the flight. Further steps were similar to the engine bay analysis, i.e., first simulations without and then with thermal radiation were carried out.

The spatial mesh for the nacelle cooling and ventilation consisted of over 11.7 million tetrahedral elements and was refined close to the boundaries especially near small elements, hot surfaces and in the gap between exhaust

pipes and exhaust pipe covers. The tetrahedral dominated meshes refined to the surfaces were also generated for simulations of thermal interaction of exhaust jets with the airplanes skins. For the I-23 the respective meshes consisted of 1.97, 14.51, and 13.41 millions elements for the exhaust pipe, on the ground and in the flight simulations, while for the EV-55 meshes were made of 0.46 and 16.05 million elements for the exhaust pipe and the exhaust jet-airplane skin interaction simulations, respectively. The quality of these spatial meshes was found to be within the acceptable range, e.g., the aspect ratio below 40, the orthogonality above 0.2 and the skewness below 0.8. The dimensionless distance from the wall to the central node of the first mesh element y^+ on the surfaces which were important from the point of view of thermal analysis, e.g., for the nacelle internal and external surface, exhaust pipes, wings, flaps and cockpit part of the fuselage were kept in the range of 30 and 1000 which is suitable for the applied wall function approach. At some surfaces where the stagnation points or flows with low velocity were observed the y^+ dropped below 30. Therefore scalable wall function was applied to avoid the deterioration of the standard wall functions under fine grid refinement.

During calculations with thermal radiation the angular grids which were required for the solution of radiative transfer equation were created with the following parameters [9–11]. For the engine bay simulations the θ, ϕ, θ pixel and ϕ pixel divisions were: $N_\theta = 4$, $N_\varphi = 8$, $N_{\theta,p} = 5$ and $N_{\phi,p} = 5$, respectively. For the flow over the airplanes the respective divisions were assumed to be: $N_\theta = 4$, $N_\varphi = 4$, $N_{\theta,p} = 5$ and $N_{\theta,p} = 5$, while for their exhaust system simulations of these airplanes a fine angular mesh were used: $N_\theta = 4$, $N_\varphi = 8$, $N_{\theta,p} = 5$ and $N_{\phi,p} = 5$.

For all considered cases the solution procedure was similar and can be described as follows. The momentum and pressure fields were coupled with the SIMPLEC algorithm [9]. Thermal radiation was modelled with the finite volume method for radiative heat transfer [10–12]. Additionally, the second order upwind scheme was applied to all equations. The radiative transfer equation was solved every 5 or 10 iterations of heat and fluid flow equations to speed up calculations. The convergence criteria for all equations were set to 10^{-4}. Moreover, in the engine bay analysis both thickness and anisotropic thermal properties of the nacelle walls were accounted for by applying 1D shell conduction model, which included transverse and planar heat conduction. This allowed to avoid generation of an unnecessary large mesh as in the geometrical model the thickness of these walls was

assumed to be infinitely thin.

Considered thermo-fluid problems were quite unique with the geometries of airplanes developed within the ESPOSA project. Therefore, the literature is lacking the reference data for verification or validation of the presented models. In this situation, only grid size studies could be performed. For each of the analysed cases additional two spatial meshes (the finest and coarsest) were prepared. Then several simulations were carried out and showed that results were grid size independent. Analysis of influence of y^+ on the results was not conducted.

4 Simulations of the nacelle cooling and ventilation in the simple-engine airplane

The aim of these simulations was to find temperature distribution and locations of hot spots on the nacelle, to assess possibility of thermal destruction of the cowling and if necessary to propose solution which will decrease temperature on the nacelle of the I-23. For more details refer to [3,5].

Table 1: Parameters of the honeycomb structure and solid material.

Parameter	Honeycomb structure	Solid material
Thickness [m]	0.00572	0.00096
Transverse thermal conductivity [W/m/K]	0.270	0.544
Planar thermal conductivity [W/m/K]	0.930	0.930
Density [kg/m^3]	2550.0	1890.0
Specific heat [J/kg/K]	884.0	884.0

Initially, the cowling was assumed to be made of honeycomb structure composite which properties are given in Tab. 1. Preliminary numerical simulations revealed dangerous hot spots just above the engine with temperature at the internal surface of the nacelle close to the maximal allowable one for this honeycomb structure. Therefore, a new construction of the top part of the nacelle was proposed in which the front part where hot spot was located was made of solid material, while the rear one where lower temperature was observed was made of honeycomb structure – see Fig. 3. As a consequence of higher thermal conductivity and lower wall thickness of the solid material than the honeycomb structure (see Tab. 1, resulting

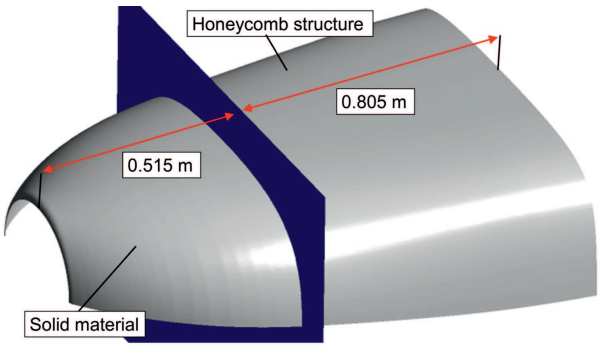

Figure 3: Final structure of the top part of the nacelle of the single-engine airplane.

thermal resistance for the solid material was lower than for the honeycomb structure) the value of maximum temperature on the internal side of nacelle was decreased (e.g., from 431.3 K to 367.7 K for flight conditions at 3000 m), while on the external side was increased (e.g., from 304.1 K to 330.1 K). Moreover, temperature distribution along the new nacelle wall resulted in lower thermal stresses in the hot spot region as gradients of temperature in the nacelle were smaller for solid material than honeycomb structure.

Contours of temperature on the internal surfaces of the modified nacelle and temperature plots along the top surface of nacelle for three cross-sections (through centreline and 0.05 m left and right from the centerline) are presented in Fig. 4 for the climbing airplane (Fig. 4A) and for the cruising altitude and speed (Fig. 4B). The hot spot is visible just above the hottest part of the engine – over the exhaust system. The highest values of temperature were equal to 376.3 K and 367.7 K for case A and B, respectively. These values were below maximal allowable temperature for the solid material and honeycomb structure.

5 Exhaust jet simulation

The aim of these simulations was to find temperature distribution and locations of hot spots on the airplanes skin, to assess possibility of thermal destruction of the airplane cover and if necessary to propose a modification which will decrease temperature on the airplane skin. For more details see [6,7].

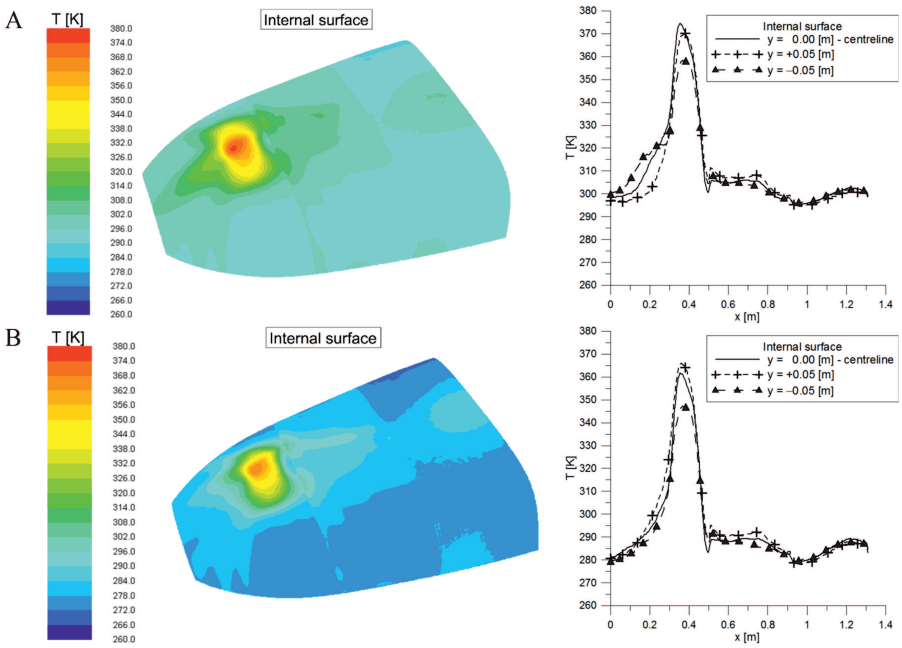

Figure 4: Contours and plots of temperature on the internal surface of the top part of the nacelle of the I-23 for: A) the climbing airplane and B) the cruising altitude and speed.

5.1 Airplane I-23

Simulations for the I-23 were performed for the airplane waiting for the take-off with landing gear fully extended (case A – sea level International Standard Atmosphere, ISA, and case B – sea level ISA + 30 K – see Fig. 5) and additionally for two velocities of its operation in the flight configuration with the landing gear retracted (case C – landing/take-off speed at altitude of 100 m and case D – cruising speed at 3000 m – see Fig. 5) – for more details regarding the simulations setup see [6,7].

Temperature distributions in two planes perpendicular to the flow direction are presented in Fig. 5 for all cases. The planes 1 and 2 are located downstream from the spinner tip at 1.6 and 3.1 m, respectively. The exhaust pipes direct the streams of hot gases below the fuselage. The exhaust gases do not directly impinge on the airplane skin for any of the analysed cases. If the speed of airplane increases streams move closer to the airplane but still there is a gap of cold air between them and the bottom part of aircraft skin. The core flow region with the highest temperature of ex-

haust gases is very small compared to the size of airplane envelope. The cross-section area of hot gases increases along the flow direction but their temperature rapidly falls down due to intensive mixing with the external cold air. About 1.0 to 1.5 m from the exhaust outlets the temperature of exhaust gases decreased by a factor of two. This process is faster for cases C and D than for A and B due to higher speed of the external air flowing round the fuselage.

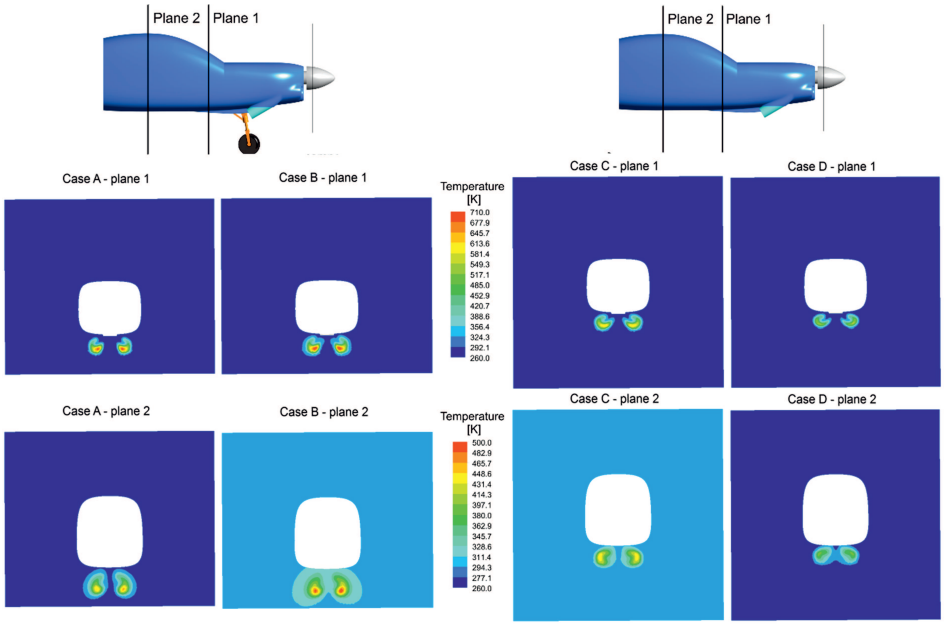

Figure 5: Temperature distributions in two planes perpendicular to the flow for: cases A and B – airplane at the ground with landing gear extended and cases C and D – airplane in flight with landing gear retracted.

Temperature distributions at the bottom part of fuselage for all considered cases are presented in Fig. 6. Despite no direct contact of hot gases with the airplane body the skin temperature at the bottom part increases. The highest temperature is observed close to the exhaust outlets and in the rear part of the computational domain. The first hotter region is mainly caused by radiative heat transfer from hot gases and hot sleeves (covers of the exhaust pipes). The second region is mainly the effect of convective heat transfer. If the external air velocity increases the temperature of the nacelle decreases as a result of more intensive cooling due to the forced convection. Additionally, Fig. 6 presents temperature plots at the bottom

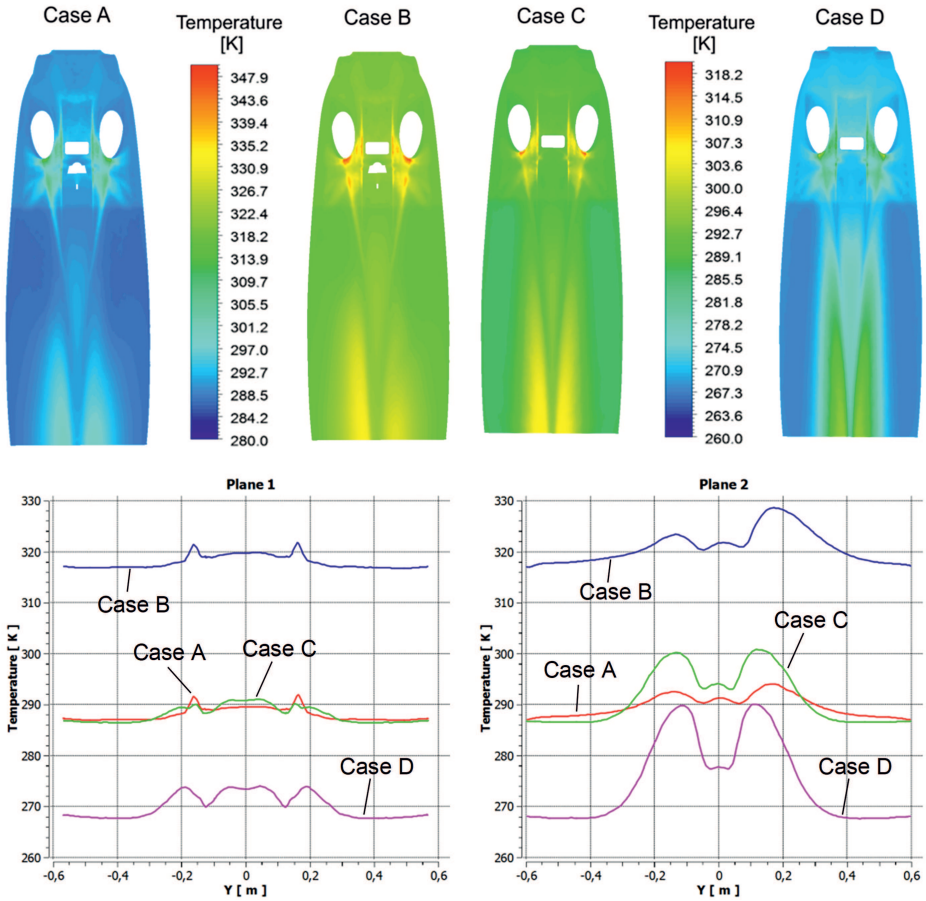

Figure 6: Contours of temperature at the bottom of the nacelle and cockpit and temperature plots along lines generated by intersection of bottom airplane skin with planes 1 and 2 (see Fig. 5).

of nacelle and cockpit along lines generated by intersection of the airplane skin with the planes 1 and 2 (see Fig. 5). It should be noticed that temperature distribution is not symmetrical. This is especially pronounced for the ground simulation due to non-symmetrical geometry of landing gear which destroys the symmetry of the flow.

The maximal values of temperature at the engine bay part of the nacelle were equal to: 320.2, 351.7, 322.9, and 305.8 K for case A, B, C, and D, respectively while the temperatures in the cockpit part of the fuselage were: 299.9, 333.0, 307.0, and 296.6 K, respectively. These values of temperatures

are far below the maximal allowable temperature of the material of the airplane skin (433 K). Therefore, no modifications of the initial geometry of the exhaust outlets were recommended for the I-23.

5.2 Airplane EV-55

As the second airplane the configuration of EV-55 was considered. Simulations were performed for the airplane waiting for take-off (case A – sea level ISA) and for cruising speed at 3000 m (case B) with flaps up (at angle 20°). Additionally, reverse conditions during landing were taken into account, with fully extended flaps (40°), for two configurations of the exhaust pipe, nominal one (case C – sea level ISA), and modified (case D – sea level ISA). More details of the simulations setup the reader can find in [6,7].

Temperature distributions in the vertical cross section through the axis of the engine nacelle are presented in Fig. 7. At the standard operating mode, like waiting for the take-off (case A) or cruise speed (case B), flaps were at high position, i.e., at angle 20°, and no considerable interactions of the stream of hot exhaust gases with the airplane, wing or flaps skin were observed. At high speeds (case B) the hot gases were additionally vigorously mixed with ambient air, so the interaction is additionally reduced with respect to the case A. During landing flaps were lowered to position of 40° and after touch down the reverse mode was activated. In this airplane configuration evident interaction of the hot gases with the wing and flaps was observed (Fig. 7, case C). The stream of hot gases was partially reversed towards the flaps mounting. Considerable temperature increase of the wing skin was observed (Fig. 8, case C), as high as 575 K, much higher than the maximum allowable temperature for the wings skin material. This could overheat the flaps skin and seriously ruin the flaps structure. As a remedy, the slight, 5° downwards rotation of the exhaust pipe was proposed in reference to the initial geometry. The temperature distribution in the vertical plane for the updated case is shown in Fig. 7, case D. For the modified geometry only slight interaction of the hot exhaust stream with the flaps was visible and the high temperature core was moved away from the airplane skin. This resulted in the considerable reducing of temperature on the wing and flaps (Fig. 8), where the maximum temperature did not exceed 370 K.

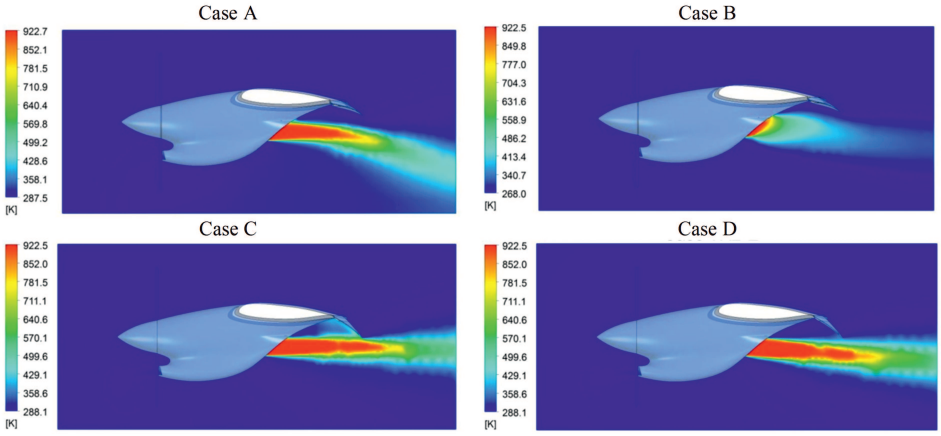

Figure 7: Contours of temperature in the vertical cross section of the nacelle for all considered cases.

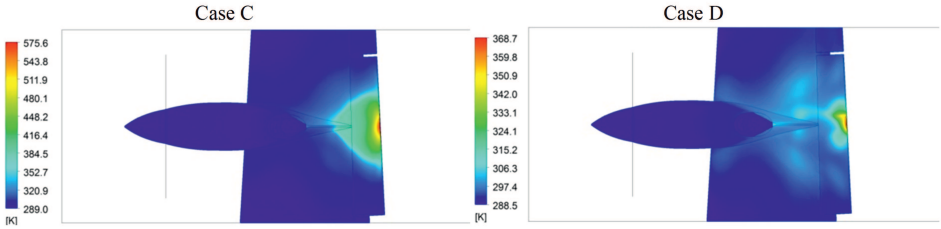

Figure 8: Contours of temperature at the engine nacelle and wing skin for cases C and D.

6 Conclusions

The paper presents analyses of heat and fluid flow in the nacelle and engine bay of the single-engine airplane I-23 and investigations of thermal interactions of streams of hot exhaust gases with the skin of the twin-engine airplane I-23 and twin-engine airplane EV-55. Both airplanes were equipped with new turboprop units during upgrade processes. Numerical models which included heat conduction and convection as well as thermal radiation were developed with the aid of the commercial software. Simulations were carried out for different operation conditions and airplanes configurations, i.e. airplanes on ground waiting for take-off and with reversed mode during landing, in flight during approach/take-off and at course altitude.

Simulations of heat transfer in the nacelle and engine bay of the single-engine airplane revealed hot spots on the cowling just above the power unit.

The value of temperature on the nacelle approached the maximal allowable temperature for its material. Therefore, a modification of the initial nacelle cover design was proposed which led to decrease in the maximal temperature value. Moreover, analyses of interaction of the streams of hot exhaust gases with the bottom part of the fuselage of the airplane showed no thermal problems and no danger of destruction of the airplane skin.

The thermal analysis of interaction of the hot exhaust gases with engine nacelle, wing and flaps of the twin-engine airplane, revealed safe temperature distribution on the skin for the standard operating mode, where flaps were at their upper position, namely at angle of 20°. The second set of considered cases correspond to configuration at which the flaps were in their lowest position, i.e., at angle of 40°. This configuration is used, e.g., for a short time period during landing, when the reverse engine mode is on after the touch down. For this case and the nominal geometry of the exhaust pipe, temperature at the flaps skin rises considerably, exceeding the maximal allowable temperature due to direct contact of the exhaust stream with flaps. As a remedy a change of the exhaust pipe geometry was proposed. The outlet pipe was rotated 5° downwards with respect to its inlet. The resulting maximum temperature at the flaps was then remarkably reduced to the safe level.

Acknowledgments This work was a part of ESPOSA Project supported by the EU within the 7 Frame Program as well as received funding from the the Faculty of Power and Aeronautical Engineering of Warsaw University of Technology in the framework of statutory activity.

Received 18 December 2017

References

[1] Goetzendorf-Grabowski T.: *Formulation of the optimization problem for engine mount design – tractor propeller case.* Aircr. Eng. Aerospa. Tec. **86**(2014), 3, 228–233.

[2] Żółtak J., Stalewski W.: *The preliminary design of the air-intake system and the nacelle in the small aircraft-engine integration process.* Aircr. Eng. Aerospa. Tec. **86**(2014), 3, 250–258.

[3] Łapka P., Seredyński M., Furmański P., Dziubiński A., Banaszek J.: *Simplified thermo-fluid model of an engine cowling in a small airplane.* Aircr. Eng. Aerospa. Tec. **86**(2014), 3, 242–249.

[4] Iwaniuk A., Wisniowski W., Zóltak J.: *Multi-disciplinary optimisation approach for a light turboprop aircraft-engine integration and improvement.* Aircr. Eng. Aerospa. Tec. **88**(2016), 2, 348–355.

[5] Łapka P., Bakker M., Furmanski P., van Tongeren H.: *Comparison of 1D and 3D thermal models of the nacelle ventilation system in a small airplane.* Aircr. Eng. Aerospa. Tec. **90**(2018), 1, 114–125.

[6] Łapka P., Seredyński M., Furmański P.: *Numerical analysis of the exhaust jet in the small aircrafts.* In: Proc. 9th Int. Conf. Computational Heat and Mass Transfer, ICCHMT 2016, Cracow, 23-26 May 2016, 202, 1–11.

[7] Łapka P., Seredyński M., Furmański P.: *Investigation of thermal interactions between the exhaust jet and airplane skin in small aircrafts.* Prog. Comput. Fluid Dy. (2017), (accepted for publication).

[8] Łapka P., Seredyński M., Ćwik A.: *Preliminary study on supercritical hydrogen and bleed air heat exchanger for aircraft application.* Proc. Inst. Mech. Eng. G: J. Aerospace Eng. **232**(2017), 12, 2231–2243., https://doi.org/10.1177/0954410017711723

[9] Versteeg H.K., Malalasekera W.: *An Introduction to Computational Fluid Dynamics.* Pearson Education, Harlow 2007.

[10] Howell J.R., Siegel R., Mengüç M.P.: *Thermal Radiation Heat Transfer.* CRC Press, Boca Raton 1992.

[11] Łapka P., Furmański P.: *Fixed grid simulation of radiation-conduction dominated solidification process.* J. Heat Trans. **132**(2010), 2, 023504.

[12] Łapka P., Furmański P.: *Fixed Cartesian grid based numerical model for solidification process of semi-transparent materials I: modelling and verification.* Int. J. Heat Mass Tran. **55**(2012), 19-20, 4941–4952.